Injection-induced bifurcations of transverse spatiotemporal patterns in semiconductor laser arrays

D. Merbach,[1] O. Hess,[2] H. Herzel,[1] and E. Schöll[1]
[1]*Institut für Theoretische Physik, Technische Universität Berlin, Hardenbergstraße 36, D-10623 Berlin, Germany*
[2]*Institut für Technische Physik, Deutsche Forschungsanstalt für Luft- und Raumfahrt, Pfaffenwaldring 38-40, D-70569 Stuttgart, Germany*
(Received 1 February 1995)

We present results of numerical investigations on the complex spatiotemporal dynamics of semiconductor laser arrays. The diffusion of charge carriers turns out to be essential for instabilities in the output intensity above the laser threshold. Besides other bifurcations, a period doubling of a torus is found. The Karhunen-Loeve decomposition gives the dominant modes of the spatiotemporal dynamics of the output intensity and provides a measure of the number of spatiotemporal degrees of freedom.

PACS number(s): 05.45.+b, 42.50.Ne, 42.55.Px

I. INTRODUCTION

Self-organized transverse spatiotemporal patterns arise in a variety of nonlinear optical systems, especially lasers [1–3]. Of particular current interest are arrays of semiconductor injection lasers, where several laser oscillators are combined in a single device on one substrate.

Describing the dynamics of semiconductor laser arrays within the framework of the coupled mode theory may reveal a number of fundamental properties [4]. For instance, it predicts that the emitters of the array oscillate collectively in modes of the composite waveguide. These so-called supermodes have been experimentally observed [5]. Thus in most studies on the dynamic behavior of semiconductor laser arrays, where rate equations are used for the electric field and the carrier density [6], the coupling of the electric field of adjacent lasers is described by a scalar coupling coefficient, and the diffusion of charge carriers is neglected since it cannot be easily included in the coupled mode description based on ordinary differential equations. However, it has recently been realized that it is the combination of the dynamically and spatially varying optical coupling via diffraction with the time dependent transverse diffusion of the charge carriers between the laser stripes which is responsible for a striking complexity in the dynamics of the array [7–10].

In this paper we present results of our numerical investigations of the dynamics of transversely coupled semiconductor lasers on the basis of a phenomenological laser model involving partial differential equations [7,9]. The variation of the injection current leads to different coupling situations with complex spatiotemporal dynamics. We study the various dynamic regimes by analyzing the output intensity and the charge carrier density with methods from nonlinear dynamics. Our investigations extend and complement previous studies on twin-stripe semiconductor lasers [9,11]. Here we consider three-stripe and ten-stripe arrays. The results of our extensive numerical simulations not only show interesting dynamic bifurcation phenomena but, as we will demonstrate in the following, also help to shed some light on the internal dynamic coupling mechanisms in semiconductor laser arrays. In particular, by deliberately neglecting diffusion—in direct comparison with the "normal" case where carrier diffusion is correctly taken into account—we qualitatively determine the influence which nonlinear coupling by the transversely diffusing charge carriers have on the dynamical behavior of the array.

We will proceed along the following line: In Sec. II we briefly present the model under consideration. The influence of particle diffusion on the dynamical behavior and the bifurcations leading to chaotic oscillations of the output intensity are described in Sec. III. In Sec. IV we focus on the quantitative analysis of spatiotemporal patterns, by means of the Karhunen-Loeve decomposition. Finally, Sec. V summarizes our findings and draws some conclusions.

II. THE MODEL

A typical semiconductor laser array is schematically shown in Fig. 1. The laser structure essentially consists of a $GaAs/Al_xGa_{1-x}As$ heterostructure, with GaAs being the active layer. Current is injected through the contact stripes at the top of the device. The stripe width of $w = 5.0\,\mu m$ is chosen such that one stripe can support one transverse optical mode. The stripes are separated by a distance of $s = 5.8\,\mu m$ from each other. The heterostructure vertically (in the y direction) confines the charge carriers to the active layer. In the transverse (x) direction, however, not only can the carriers freely diffuse but also the optical field-modes of each stripe overlap, leading to the aforementioned dynamic twofold coupling mechanism between the individual lasers.

The model equation for the electric field E is based on Maxwell's wave equation in paraxial approximation. Due to the difference in refractive indices between the layers of GaAs and $Al_xGa_{1-x}As$, the optical field is vertically (in the y direction) confined to the active layer. As the heterostructure is thin enough to support only one mode in the y direction, its waveguiding properties can be de-

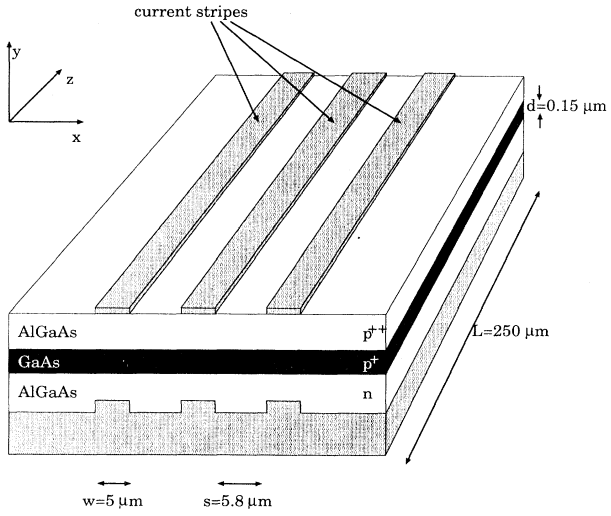

FIG. 1. Setup of a three-stripe laser. The middle layer (GaAs) of the double heterostructure is the active region. The charge carriers are injected through the contact stripes at the top of the device.

scribed in the steady state. By means of the effective index approximation they can be represented as transversely dependent parameters. Averaging with respect to the longitudinal (z) direction leads to a mean field model which depends on one dimension in space denoted by x. Adiabatically eliminating the polarization variable, the interaction of the electric field and the semiconductor material is phenomenologically described by a linear gain function $g(N) = aN - b$ and by the linewidth enhancement factor α. The dynamics of the charge carrier density N is governed by a diffusion equation (diffusion constant D_f) including the pump term Λ which models injection of carriers, and $\gamma_{\rm nr}$ represents the nonradiative recombination coefficient. The dynamic equations are given by

$$\frac{n_l}{c}\frac{\partial}{\partial t}E = iD_p\frac{\partial^2}{\partial x^2}E - [\gamma_m + i\eta(x)]E + \Gamma(x)[g(N) - i\alpha aN]E, \tag{1a}$$

$$\frac{\partial}{\partial t}N = D_f\frac{\partial^2}{\partial x^2}N - \gamma_{\rm nr}N + \Lambda(x) - \frac{2\epsilon_0 c}{\hbar\omega n_l}g(N)|E|^2. \tag{1b}$$

The first term on the right-hand side of Eq. (1a) describes the coupling of adjacent lasers by diffraction, where $D_p = (2n_l k_0)^{-1}$ is the diffraction coefficient with vacuum wave number $k_0 = 2\pi/\lambda$, λ being the optical wavelength and n_l the refractive index of the active layer. Resonator losses due to the mirror transmissivity are included in the constant $\gamma_m = -\ln\sqrt{R_1R_2}/2L$; R_1 and R_2 are the reflectivities of the two facets and L is the length of the laser. Passive waveguiding properties are represented by $\eta(x)$ which results from the effective index approximation. The variation in confinement of the vertical mode profile due to the ribbed transverse structure is described by the confinement factor Γ. The parameters ϵ_0, c, and ω are the absolute permittivity, vacuum velocity of light, and frequency, respectively. The pumping term $\Lambda(x)$ vanishes between the stripes and has a value of $\eta_i J/(edwL)$ underneath the stripes with the total injection current per stripe J, where e, d, and η_i are the elementary charge, the thickness of the active layer, and the injection efficiency, respectively.

Equations (1b) have to be supplemented by the transverse boundary conditions $\partial E/\partial x = \mp\alpha_w E$ and $\partial N/\partial x = \mp\alpha_{sr}N$ at the two transverse sides, where α_w is the surface absorption constant, and α_{sr} is the surface recombination constant. The optical output intensity at the front facet is given by $I(x,t) = (1 - R_1)\epsilon_0 c/n_l\,|E(x,t)|^2$.

The model equations (1b) are discretized and numerically solved using the hopscotch method [7]. The parameter values used in the simulations are listed in Table I.

III. BIFURCATION SCENARIOS WITH AND WITHOUT DIFFUSION

Pumping an array of three-stripe lasers just above its lasing threshold (with the parameters listed in Table I we find a threshold current $J_{\rm th} = 36\,$mA per stripe) results in a continuous emission of light: the lasers are not coupled and reach a steady state [Fig. 2(a)] after a few relaxation oscillations. Increased injection current causes stronger coupling of the fields and leads to self-sustained relaxation oscillations with typical frequencies of a few GHz. These oscillations may be periodic [Fig. 2(b)] or quasiperiodic with two [Fig. 2(c)] or more [11] incommensurate frequencies. Further increase of the pump-

TABLE I. Semiconductor laser parameters.

L	$= 250\,\mu$m	Cavity length
w	$= 5.0\,\mu$m	Stripe width
s	$= 5.8\,\mu$m	Stripe separation for the three-stripe laser
s	$= 5.0\,\mu$m	Stripe separation for the ten-stripe laser
d	$= 0.15\,\mu$m	Thickness of active layer
R_1	$= 0.99$	Reflectivity of first mirror
R_2	$= 0.32$	Reflectivity of second mirror
λ	$= 815\,$nm	Laser wavelength
n_l	$= 0.59$	Refractive index of active layer
n_c	$= 0.32$	Refractive index of cladding layer
a	$= 1.5 \times 10^{-16}\ \mathrm{cm}^2$	Linear gain coefficient
b	$= -1.0 \times 10^2\ \mathrm{cm}^{-1}$	Linear loss coefficient
D_p	$= 18 \times 10^{-6}\,$m	Diffraction coefficient
D_f	$= 30\,\mathrm{cm}^2\,\mathrm{s}^{-1}$	Diffusion coefficient
$\gamma_{\rm nr}$	$= 2 \times 10^8\,\mathrm{s}^{-1}$	Nonradiative recombination coefficient
Γ	$= 0.5014$	Confinement factor below stripes
	$= 0.5149$	Confinement factor between stripes
η_i	$= 0.5$	Efficiency of injection
α_w	$= 30\,\mathrm{cm}^{-1}$	Surface absorption constant
α_{sr}	$= 10^8\,\mathrm{cm\,s}^{-1}$	Surface recombination constant

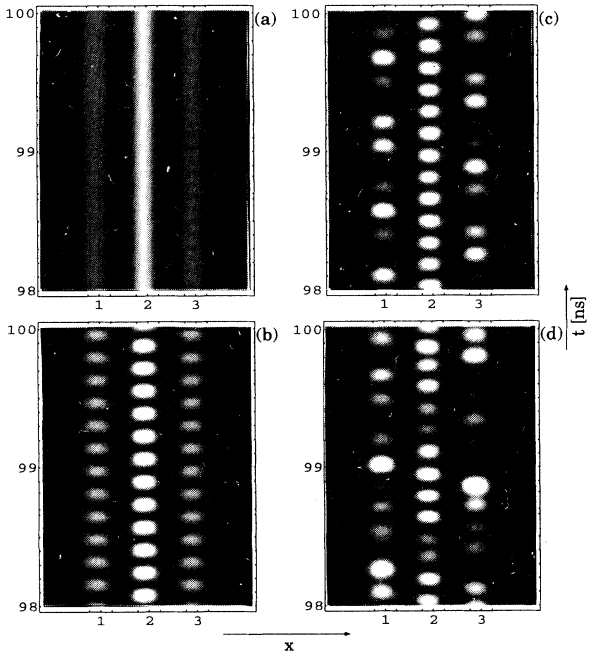

FIG. 2. Gray scale plot of the spatiotemporal output intensity of the three-stripe laser array for four different injection currents J. Bright colors represent high intensity values, dark shading indicates low intensity. (a) $J = 40.8$ mA: continuous wave, (b) $J = 44.6$ mA: periodic, (c) $J = 50.0$ mA: quasiperiodic (two-torus), (d) $J = 60.0$ mA: chaotic.

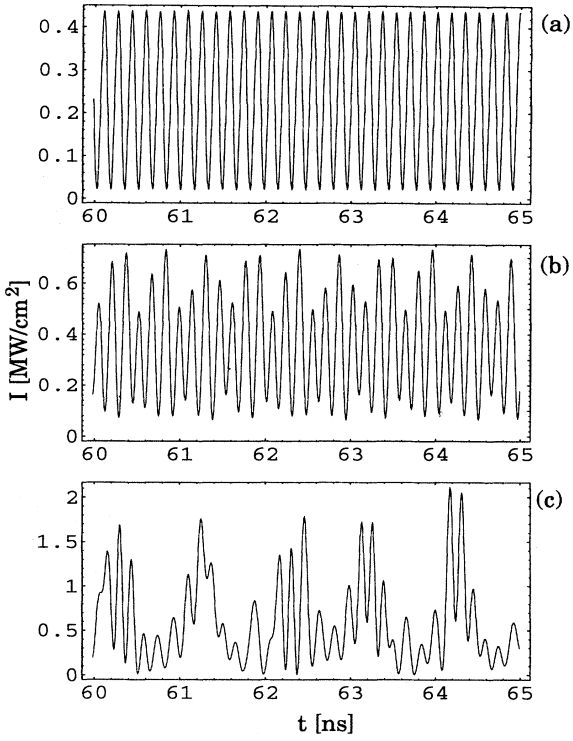

FIG. 3. Time series of the output intensity in the center of the middle stripe. (a) $J = 44.6$ mA: periodic, (b) $J = 50.0$ mA: quasiperiodic, (c) $J = 60.0$ mA: chaotic.

ing strength enhances the already strong coupling of the lasers even more and results in a chaotically pulsating spatiotemporal intensity distribution [Fig. 2(d)]. The plots in Fig. 3 showing time trace cuts of the spatiotemporal distribution again pertain to these situations. The time series of the output intensity I in the center of the middle stripe in Fig. 3(a) is periodic, whereas it is quasiperiodic in Fig. 3(b) and chaotic in Fig. 3(c). The power spectra of the time series reveal the various frequencies involved, and support the strong broad-band irregularity of the optical signal as shown in Fig. 3(c). In the following we will use the logarithmic power spectra of the intensity of the middle laser stripe to identify the various regimes involved in the dynamics of the three-stripe laser. Using spectral analysis the bifurcations upon variation of the injection current J are comprehensively visualized in Fig. 4. This figure presents the results of extensive numerical simulations by giving an overview of the frequencies excited in the temporal variation of the output intensity. Logarithmic power spectra of the intensity of the middle laser stripe are graphically shown in the form of a density plot versus the injection current. Figure 4(a) is attained with the diffusion coefficient having the realistic value of $D_f = 30$ cm^2/s, whereas in the corresponding simulations pertaining to Fig. 4(b) the diffusion coefficient has been reduced by 6 orders of magnitude to $D_f = 3 \times 10^{-5}$ cm^2/s. Generally, we identify discrete power spectra for the periodic and quasiperiodic regimes. For time series showing chaotic dynamical behavior, the power spectra are quasicontinuous. The direct comparison of Fig. 4(a) with Fig. 4(b) gives a clear indication of the importance of diffusive coupling effects. In fact, in a large regime of physically relevant values of the pumping strength an imaginary diffusionless three-stripe semiconductor laser array would oscillate in a stable mode. This is in striking contrast to the realistic laser array where instabilities appear. Evidently carrier diffusion is a fundamental mechanism involved in the emergence of instabilities in semiconductor lasers arrays. Therefore, transverse diffusion should clearly not be neglected as opposed to many common theoretical and numerical studies.

Zooming in on a particularly interesting part of Fig. 4(a), we now focus on the bifurcations leading from the fixed point just above the laser threshold to the chaotically pulsating intensity. In Fig. 5(a) a blow-up of the relevant region in Fig. 4 is shown, revealing a considerable substructure in the bifurcations. The first Hopf bifurcation occurs at a pumping strength of $J = 41$ mA, which is 1.14 times the laser threshold. A secondary Hopf bifurcation is found around $J = 45$ mA which corresponds to 1.25 times the threshold current. The output intensity becomes quasiperiodic with two incommensurate frequencies. After further bifurcations the dynamics turns to chaotic behavior above $J = 52$ mA. As shown in Figs. 5(b)–(e) these bifurcations are associated with changes of mean values and standard deviations of the intensity. At the secondary Hopf bifurcation not only is a new frequency being introduced but at the same time the oscil-

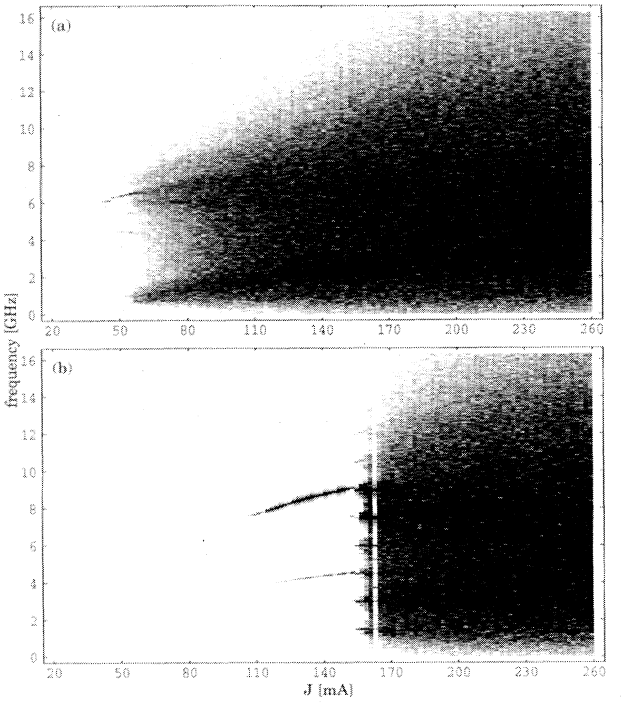

FIG. 4. Frequency bifurcation diagrams. The logarithmic power spectra are shown as a density plot vs the injection current J per stripe. Dark color corresponds to high amplitudes. (a) With correct diffusion coefficient $D_f = 30$ cm^2/s, (b) With reduced diffusion coefficient $D_f = 3 \times 10^{-5}$ cm^2/s. For each value of J the power spectrum is calculated for the time interval from $t = 38.6$–100 ns corresponding to 8192 data points.

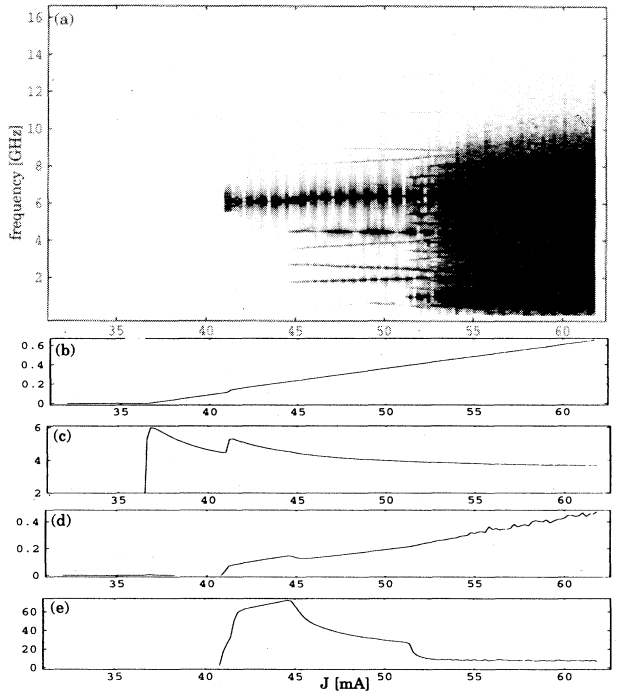

FIG. 5. (a) Blow-up of the frequency bifurcation diagram of Fig. 4(a). (b) Temporal average of the intensity in the center of the middle stripe in MW/cm^2, (c) temporal average normalized to the total intensity (averaged in time and space), (d) standard deviation of the intensity in the center of the middle stripe in MW/cm^2, (e) standard deviation of the intensity in the center of the middle laser stripe normalized to the standard deviation of the transversely averaged intensity.

lation strength is changed considerably. This can be seen in Fig. 6 showing the time series of the output intensity at the centers of the three laser stripes excited just above the second Hopf bifurcation. At this point, the limit cycle has lost its stability and a torus is approached after a long transient. Note that due to diffusion of carriers into the absorbing edges of the array the output intensity of the middle stripe is higher than the corresponding values of the left or the right stripe. For the limit cycle regime, the oscillation strength of the left and right stripes is considerably less than that of the middle one. With the occurrence of the second frequency the oscillation strength of the left and right stripes increases to the order of the oscillation strength of the middle stripe, whereas the variance of intensity of the middle stripe is slightly reduced. These changes can be seen in Figs. 5(b)–5(e) which show the time average and the standard deviation of the middle laser stripe. The mean value (temporal average) of the output intensity in the center of the middle laser stripe displayed in Fig. 5(b) reflects—by its linear dependence on the pumping current J above the threshold $J_{\text{th}} = 36$ mA—the linear approximation in the semiconductor gain function, where, e.g., saturation effects at high pumping levels are disregarded. However, when plotting the ratio of the temporal mean of the intensity in the center of the *middle* stripe to the total intensity (averaged with respect to time and space) in Fig. 5(c), we observe a decrease of this ratio with increasing injection current, but more importantly, a distinct jump at the first Hopf bifurcation point. This tendency is even more highlighted in Fig. 5(d) showing the standard deviation of the output intensity of the middle stripe. Clearly, the two jumps observed in Fig. 5(d) indicate the first and the second Hopf bifurcation. Finally, in Fig. 5(e) the standard deviation of the output intensity of the center of the *middle* stripe normalized to the standard deviation of the transversely averaged output intensity is shown. The two Hopf bifurcations and the bifurcation to chaotic dynamics are clearly visible.

In our view, these sudden changes already are indications of a more complex dynamical behavior involving spatially distributed coupling between the stripes. However, before engaging on a closer analysis of the spatiotemporal correlations in Sec. IV, we will concentrate on the bifurcations in the intensity leading from the torus to chaotic dynamical behavior.

Inspection of Fig. 5(a) reveals the appearance of additional spectral peaks near the transition to chaos. Among the different routes to chaos (see [12] for a recent review)

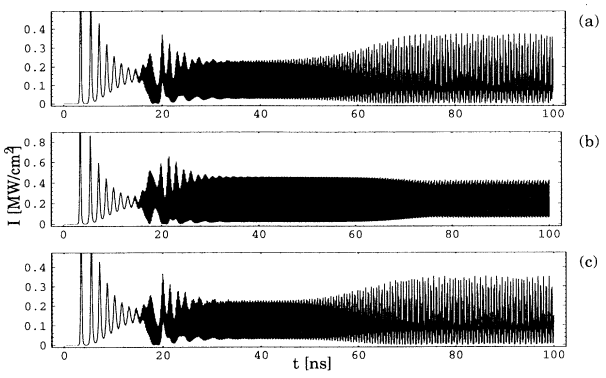

FIG. 6. A transient time series of the output intensity in the center of the respective stripe near the second Hopf bifurcation (J=44.92 mA). The stability of the limit cycle is lost, leading to a stable torus. (a) Left stripe, (b) middle stripe, (c) right stripe.

the period doubling of a torus attracted much attention during the past decade [13–16]. Theoretical considerations predict that in contrast to the period-doubling cascade of a limit cycle the torus-doubling cascade is disrupted after a few steps [17]. The subharmonics around 52 mA in Fig. 5(a) are a first indication of a torus doubling. In Fig. 7 next-maximum maps are used to resolve details of the transition. The closed curve in Fig. 7(a) reveals a torus with two incommensurate frequencies at an injection current of $J = 50.8$ mA. Increasing the pumping strength leads to a bifurcation of the torus. Torus doubling can be seen at a pumping strength of $J = 51.4$ mA,

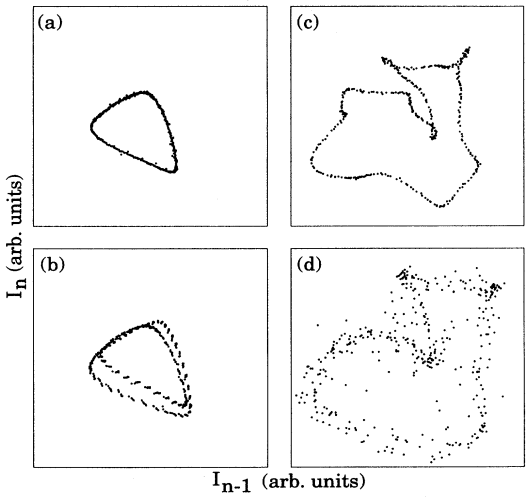

FIG. 7. Next-maximum maps of the intensity time series near the period doubling of the torus. The maxima of the intensity in the center of the middle stripe I_n are plotted versus I_{n-1}. (a) Torus, $J = 50.8$ mA, (b) doubled torus, $J = 51.4$ mA, (c) wrinkled torus, $J = 52.0$ mA, (d) destroyed torus, $J = 52.6$ mA.

with the points of the next-maximum map in Fig. 7(b) still arranged on a closed curve. With further increase of the injection current the period-doubled torus loses its smoothness [Fig. 7(c)] and results in chaotic dynamics of the output intensity [Fig. 7(d)]. The observation of just a single doubling bifurcation and subsequent loss of smoothness is consistent with numerical and theoretical studies [18,12].

IV. SPATIOTEMPORAL COMPLEXITY

Looking at the density plots of the intensity distribution in Fig. 2, our visual perception suggests—by the complexity of the patterns—that temporal and spatial degrees of freedom are simultaneously excited and seem to be intrinsically coupled. Also, when comparing the intensities of the three laser stripes in the preceding section, we found indications of a simultaneous temporal and spatial variation of the coupling between the stripes. In the following, by applying the Karhunen-Loeve decomposition [19–21] to our computed data, we are able to quantify the spatiotemporal complexity. With the help of this analysis a few relevant spatial "patterns" can be extracted and we will use these eigenmodes as basis functions to separate the spatial and temporal dynamics [22].

Let $u(x,t)$ be the quantity under consideration; then the Karhunen-Loeve expansion (or proper orthogonal decomposition)

$$u_M(x,t) = \sum_{i=1}^{M} a_i(t)\,\phi_i(x) \tag{2}$$

yields a good approximation to $u(x,t)$ in the sense of a minimal mean squared error for a given number M. The spatial functions $\phi_i(x)$ are called eigenmodes, whereas the temporal functions $a_i(t)$ are the amplitudes of the corresponding modes. The first eigenmode which fits best is determined by solving the variational problem

$$\lambda_1 = \max_{\phi_1} \left\{ \lim_{T\to\infty} \frac{1}{T} \int_0^T (\phi_1, u)^2\, dt \right\} \tag{3}$$

with $(.,.)$ being a scalar product with respect to space. The other eigenmodes are determined analogously taking into account orthogonality and normalization [19]. This variational problem is equivalent to the eigenvalue problem for the covariance matrix

$$C_{k,l} = \frac{1}{T} \int_{t_0}^{t_0+T} u(x_k,t)u(x_l,t)\, dt \tag{4}$$

expressed in terms of the discretized transverse coordinate x.

The eigenvalues λ_i corresponding to the eigenmodes ϕ_i of the covariance matrix are equal to the variance of the ith mode amplitude $\langle a_i(t)\rangle^2$ and therefore a measure of the strength of the modes involved in the dynamics. When comparing these eigenvalues it is advantageous to introduce relative eigenvalues normalized to the sum of

all eigenvalues

$$\tilde{\lambda}_i = \frac{\lambda_i}{\sum_j \lambda_j}. \tag{5}$$

To analyze the dynamics of the semiconductor laser it is appropriate to choose

$$u^I(x,t) \equiv \frac{I(x,t) - \langle I(x) \rangle}{\sqrt{\langle I(x) \rangle}} \tag{6a}$$

and

$$u^N(x,t) \equiv \frac{N(x,t) - \langle N(x) \rangle}{\sqrt{\langle N(x) \rangle}} \tag{6b}$$

as spatiotemporal quantities under consideration, where $\langle\,\rangle$ denotes the temporal average [22].

Figure 8 shows the eigenmodes of $u^I(x,t)$ corresponding to the time series in Fig. 3. The numbers indicate the relative eigenvalues $\tilde{\lambda}_i$. Obviously, periodic oscillations in time [Fig. 3(a)] are governed by only one dominant spatial mode which describes the alternating "firing" of adjacent laser stripes [Fig. 8(a)]. The left and right stripes oscillate in phase, while the intensity of the middle stripe lags by half a period. The quasiperiodic oscillations [Fig. 3(b)] are related to two relevant eigenmodes; the first mode of the periodic regime now has become the second one, whereas the new first mode describes the alternating oscillations of the left and right stripe, however not affecting the middle stripe [Fig. 8(b)]. Looking at the chaotic regime [Fig. 3(c)], a third transverse mode is excited, describing the simultaneous in-phase oscillation of all stripes [Fig. 3(c)]. (It should be noted that all modes describe the deviation of the intensity field from the time average.) Analogous to Fig. 8, Fig. 9 shows the eigenmodes of the charge carrier density. Those modes differ from the intensity modes by the fact that they are more confined to the region under the current injection stripes.

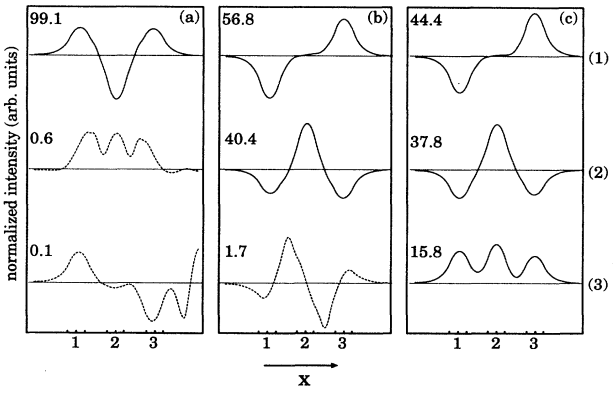

FIG. 8. Eigenmodes of the intensity field $I(x,t)$. For three different injection currents (cf. Fig. 3) the first three eigenmodes $\phi_i(x)$, $i = 1, 2, 3$ are shown, the numbers denoting their respective eigenvalues $\tilde{\lambda}_i$. Relevant modes are depicted by solid lines, very weak modes by dashed lines. (a) $J = 44.6$ mA: periodic dynamics, (b) $J = 50.0$ mA: quasiperiodic dynamics, (c) $J = 60.0$ mA: chaotic dynamics.

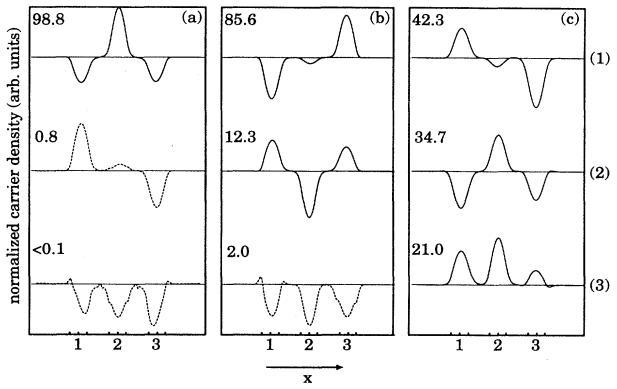

FIG. 9. Eigenmodes of the carrier density field $N(x,t)$, same plot as in Fig. 8.

The confinement is strongly influenced by the diffusion coefficient.

Figure 10 shows the output intensity of a laser array with ten elements for two different injection currents. In Fig. 10(a) the dynamics is periodic whereas in Fig. 10(b) it is chaotic. The corresponding eigenmodes are shown in Figs. 11 and 12. The periodic time series can be described by two eigenmodes containing 98% of the variance. The first mode in the periodic regime (Fig. 11) describes a modulation of the output of the ten neighboring stripes with a sinusoidal envelope of one period across the transverse direction, whereas the second mode corresponds to such a modulation with 3/2 periods. In a sense those envelopes are equivalent to the two dominant

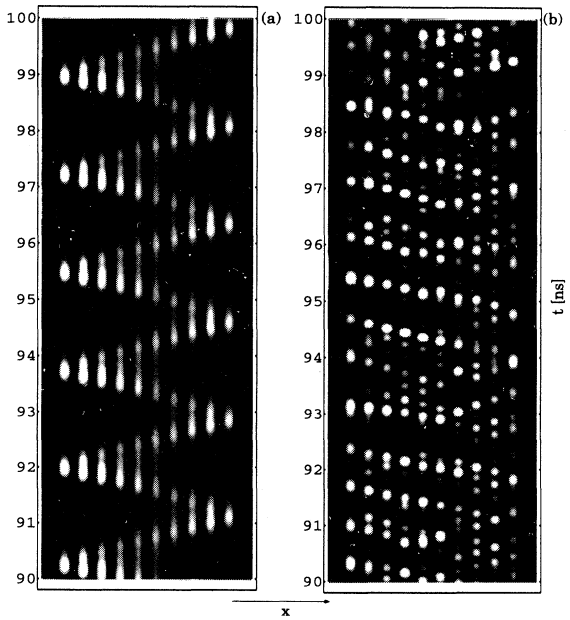

FIG. 10. Gray scale plot of the spatiotemporal output intensity of a ten-stripe laser array for two different injection currents. (a) $J = 34$ mA: periodic, (b) $J = 44$ mA: chaotic.

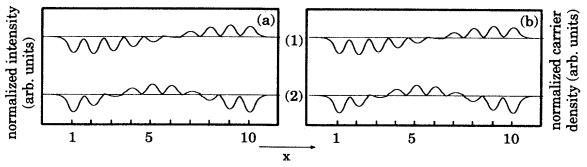

FIG. 11. Relevant eigenmodes $\phi_i(x)$ of the ten-stripe laser array for the periodic regime ($J = 34$ mA). (a) eigenmodes of the intensity field, (b) eigenmodes of the carrier density field.

eigenmodes in Figs. 8(b) and 9(b). The chaotic time series, on the other hand, requires ten modes for a correct description (they cover 97% of the variance), indicating much more complicated dynamics due to the excitation of higher spatial modes.

This can be verified in Fig. 13 where the absolute eigenvalues λ_i are shown for several injection currents, indicating the successive excitation of new modes with increased pumping strength leading from periodic oscillations to spatiotemporal chaotic dynamics. Note that even at high pumping, the number of relevant eigenmodes does not exceed 10, i.e., the number of laser stripes; such behavior is not self-evident in a spatiotemporal system.

V. CONCLUSIONS

We studied the spatiotemporal dynamics of semiconductor laser arrays based on a description in terms of partial differential equations, and have identified various dynamical regimes. Particularly, a 2-torus is stable in a wide range of parameters. At large pumping irregular spatiotemporal patterns are found. Near the transition to the chaotic regime a period doubling of a torus is found, revealed clearly by spectral bifurcation diagrams and next-maximum maps. More quantitative insight into the spatiotemporal patterns is gained by the Karhunen-Loeve decomposition. Although there are potentially thousands of degrees of freedom in a spatially extended system like the semiconductor laser, even in the strongly irregular regime of the ten-stripe laser only 10 spatial modes contain more than 97% of the dynamics as measured by the corresponding eigenvalues.

Finally, our study puts strong emphasis on the role of the charge carrier diffusion as an important coupling mechanism in addition to the overlapping of evanescent fields. It strongly influences the dynamical behavior and induces instabilities as shown by comparison with neglected diffusion.

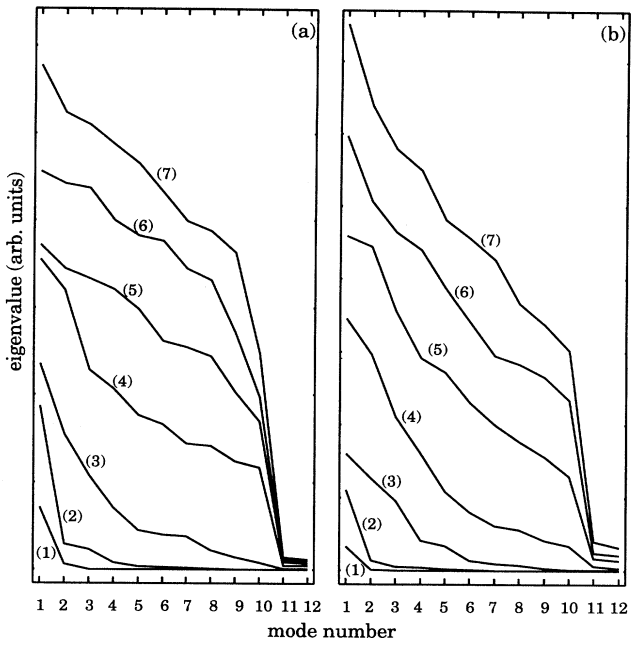

FIG. 13. Eigenvalues λ_i of the first 12 eigenmodes of the ten-stripe laser array for injection currents from (1) $J = 34$ mA to (7) $J = 58$ mA in steps of 4 mA. (a) Intensity eigenmodes, (b) carrier density eigenmodes.

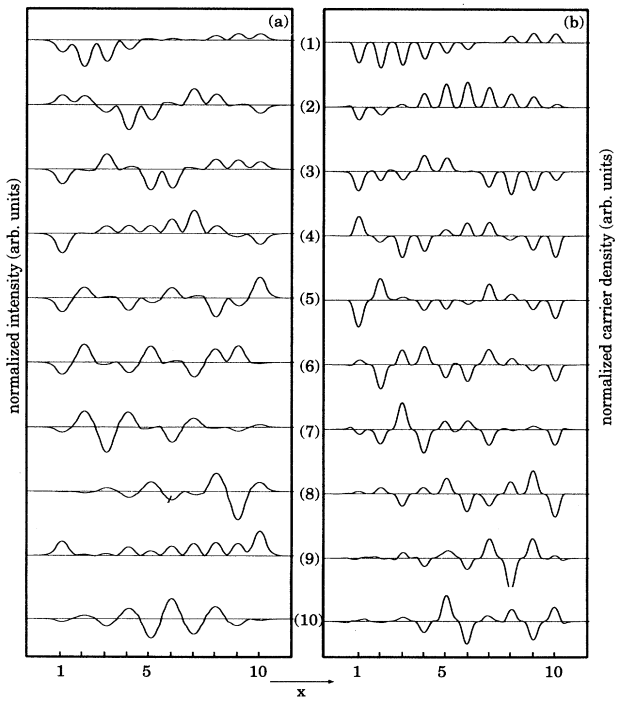

FIG. 12. Relevant eigenmodes $\phi_i(x)$ of the ten-stripe laser array for the chaotic regime ($J = 44$ mA). (a) Eigenmodes of the intensity field, (b) eigenmodes of the carrier density field.

ACKNOWLEDGMENT

Partial support by Deutsche Forschungsgemeinschaft is gratefully acknowledged.

[1] L. A. Lugiato, F. Prati, L. M. Narducci, P. Ru, J. R. Tredicce, and D. K Bandy, Phys. Rev. A **37**, 3847 (1988).
[2] N. B. Abraham and W. J. Firth, J. Opt. Soc. Am. B **7**, 951 (1990).
[3] C. O. Weiss and R. Vilaseca, *Dynamics of Lasers*, edited by H.-G. Schuster (VCH, Weinheim, 1991).
[4] J. K. Butler, D. E. Ackley, and D. Botez, Appl. Phys. Lett. **44**, 293 (1984).
[5] T. L. Paoli, W. Streifer, and R. D. Burnham, Appl. Phys. Lett. **45**, 217 (1984).
[6] S. S. Wang and G. H. Winful, Appl. Phys. Lett. **52**, 1774 (1988); H. G. Winful and S. S. Wang, *ibid.* **53**, 1894 (1988).
[7] O. Hess, *Spatio-Temporal Dynamics of Semiconductor Lasers* (Wissenschaft und Technik Verlag, Berlin, 1993).
[8] H. Adachihara, O. Hess, R. Indik, and J. V. Moloney, J. Opt. Soc. Am. B **10**, 496 (1993).
[9] O. Hess and E. Schöll, Physica D **70**, 165 (1994).
[10] L. Rahman and H. G. Winful, Opt. Lett. **18**, 128 (1993).
[11] O. Hess, D. Merbach, H. Herzel, and E. Schöll, Phys. Lett. A **194**, 289 (1994).
[12] V. S. Anishchenko, M. A. Safonova, U. Feudel, and J. Kurths, Int. J. Bifurcation Chaos **4**, 595 (1994).
[13] K. Kaneko, Prog. Theor. Phys. **69**, 1806 (1983).
[14] V. Franceschini, Physica D **6**, 285 (1983).
[15] M. R. Bassett and J. L. Hudson, Physica D **35**, 289 (1989).
[16] J. M. Flesselles, V. Croquette, and S. Jucquois, Phys. Rev. Lett. **72**, 2871 (1994).
[17] A. Arnédo, P. H. Coullet, and E. Spiegel, Phys. Lett. A **94**, 1 (1983).
[18] F. Argoul and A. Arneodo, J. Méc. Théor. Appl., numéro spécial 1984, p. 241.
[19] H. Herzel, K. Krischer, D. Berry, and I. Titze, in *Spatio-Temporal Patterns in Nonequilibrium Complex Systems*, edited by P. E. Cladis and P. Palffy-Muhoray (SFI Studies in the Sciences of Complexity, Addison-Wesley, 1995).
[20] L. Sirovich, Physica D **37**, 126 (1989).
[21] M. Caponeri and S. Ciliberto, Physica D **58**, 365 (1992).
[22] O. Hess and E. Schöll, Phys. Rev. A **50**, 787 (1994).

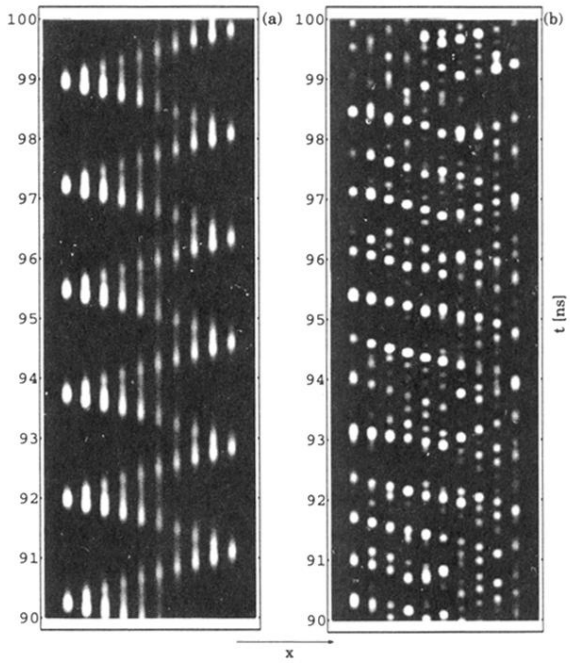

FIG. 10. Gray scale plot of the spatiotemporal output intensity of a ten-stripe laser array for two different injection currents. (a) $J = 34\,\mathrm{mA}$: periodic, (b) $J = 44\,\mathrm{mA}$: chaotic.

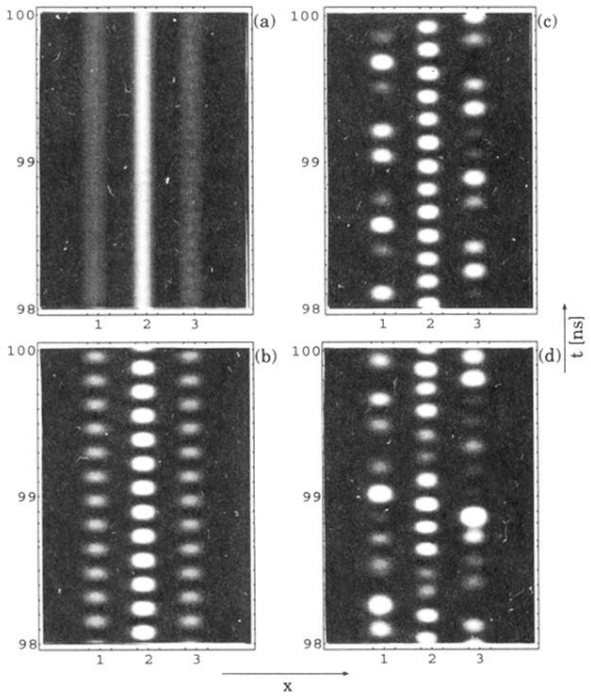

FIG. 2. Gray scale plot of the spatiotemporal output intensity of the three-stripe laser array for four different injection currents J. Bright colors represent high intensity values, dark shading indicates low intensity. (a) $J = 40.8\,\mathrm{mA}$: continuous wave, (b) $J = 44.6\,\mathrm{mA}$: periodic, (c) $J = 50.0\,\mathrm{mA}$: quasiperiodic (two-torus), (d) $J = 60.0\,\mathrm{mA}$: chaotic.

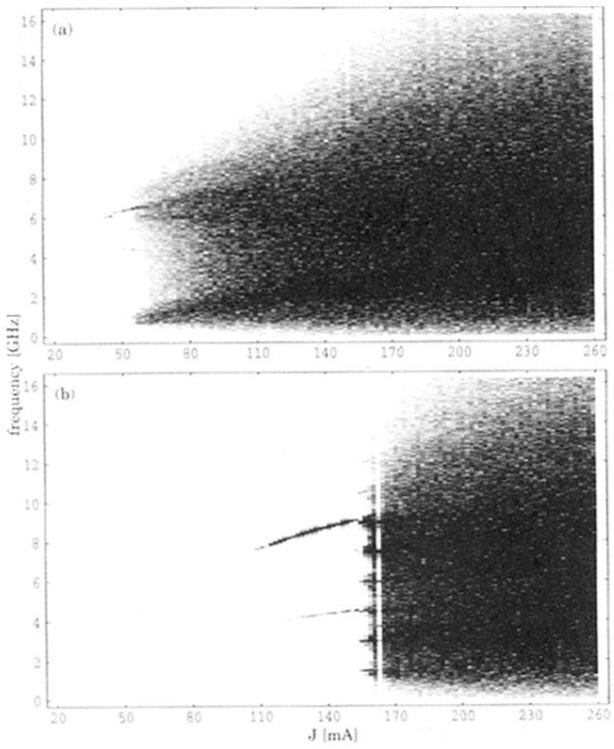

FIG. 4. Frequency bifurcation diagrams. The logarithmic power spectra are shown as a density plot vs the injection current J per stripe. Dark color corresponds to high amplitudes. (a) With correct diffusion coefficient $D_f = 30$ cm^2/s, (b) With reduced diffusion coefficient $D_f = 3 \times 10^{-5}$ cm^2/s. For each value of J the power spectrum is calculated for the time interval from $t = 38.6$–100 ns corresponding to 8192 data points.

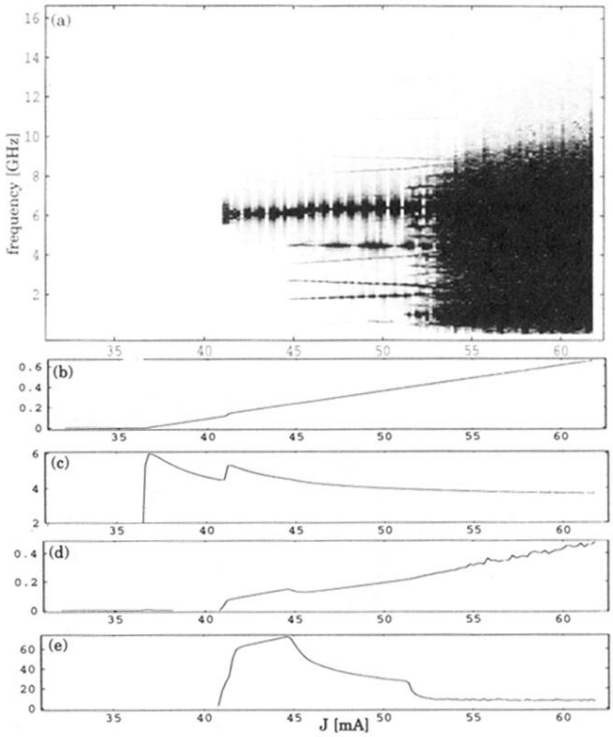

FIG. 5. (a) Blow-up of the frequency bifurcation diagram of Fig. 4(a). (b) Temporal average of the intensity in the center of the middle stripe in MW/cm^2, (c) temporal average normalized to the total intensity (averaged in time and space), (d) standard deviation of the intensity in the center of the middle stripe in MW/cm^2, (e) standard deviation of the intensity in the center of the middle laser stripe normalized to the standard deviation of the transversely averaged intensity.